This article has been accepted for publication in a future issue of this journal, but has not been fully edited. Content may change prior to final publication. Citation information: DOI10.1109/TMECH.2021.3050263, IEEE/ASME Transactions on Mechatronics

Design and validation of a novel fuzzy-logic-based static feedback controller for tendon-driven continuum robots

Weiming Ba[1], Xin Dong[1*], Abdelkhalick Mohammad[1], Mingfeng Wang[1], Dragos Axinte[1], Andy Norton[2]

***Abstract*—Continuum robots (CRs) outperform the conventional rigid-link manipulators in aspects of hyper-redundant and compliant features. They provide universal and efficient solutions to access to constrained environments, e.g., aero-engines and industrial vessels. In this paper, a slender tendon-driven continuum robot (length/diameter: 715mm/12.7mm) is introduced for in-situ maintenance of aero-engine combustors. Two control challenges, the piecewise-constant-curvature (PCC) assumption mismatch and sections coupling issues, are discussed to explain the defect of model-based kinematic controllers on specific designs. Then, inspired by the tug of war, a novel local model-less controller utilizing a fuzzy logic algorithm is proposed for the feedback control of a single section. This implements the control policies directly from the task space to the actuation space, avoiding the model mismatch of the PCC assumption owing to the explicit call of arc parameters. Experiments on a single section of the tendon-driven continuum robot, in comparison with PCC-based method, validate the stability and universality of the developed controller, which can reach $\pm$1mm overall positioning accuracy and ± 0.5mm positional accuracy for 75% of the test points in both X and Y directions. Further, a set of trails on two distal sections of a long robot demonstrate that the controller can also effectively minimise the section coupling issue.**

***Index Terms*—Continuum robot, tendon-driven, model-less static controller, fuzzy logic**

I. Introduction

Continuum robots have become essential and promising branch in the modern robot family over decades of development. Unlike rigid-link robots, composed of revolute and translation joints with high positioning accuracy and good dynamic performance, continuum robots employ compliant materials (soft material [1-3], spring [4-5], and NiTi alloy [6-7], etc.) or compliant mechanism [8-9] to construct the arm and actuators, which prevent them from rigid collisions with the surrounding environments. In addition, owing to excellent structural compliance and hyper-redundant capability, continuum robots have exhibited promising potential applicability for working in confined spaces.

Various control approaches have been proposed for the continuum robot operations, which can be classified into two major categories, i.e., open-loop and closed-loop controls. Generally, open-loop control methods are applied in the circumstances where sensor integration into the continuum arm is not applicable due to size limitations. These methods mainly rely on inverse kinematics (IK) and statics models of the continuum robots, obtained either by analysis, simulation or learning methods. For instance, reinforcement learning method with Markov Decision Process [10] was applied to learn open-loop control strategy from simulations. It achieves a mean error of 30.5mm for the position control of a 310mm long pneumatic soft manipulator. Also, a feed-forward method employing neural network was proposed to learn the inverse kinematics of a 280mm long soft robot [3]. The experiments demonstrate that the learning method outperforms the model-based Jacobian approach in terms of positional accuracy (mean error of feedforward neural network (NN): 7.35mm; that of model-based Jacobian approach: 15.12mm) owing to the fact that there are various hard-to-predict factors, e.g., friction, manufacturing and assembly errors and actuation cable discrepancy, which are difficult to be precisely modelled. Hence, for the open-loop control methods, the learning approaches work better than the model-based ones for controlling a single section continuum robot, in the aspect of control accuracy. However, when utilised for multiple-section continuum robots, the computation burden dramatically increases. Moreover, it is difficult to achieve precise control of the robot with the learning methods when variable dynamic payloads are applied to it. In terms of closed-loop control, two frameworks have been introduced for manipulating continuum/soft robots, including model-based and model-free methods. Regarding the model-based method, the PCC assumption [11-13] is still the most common kinematic model applied for the feedback control of continuum robots. For example, based on the PCC-based assumption, optimal control was employed on a 170mm-long continuum robot with two extensible modules for smooth path tracking by minimizing

*Corresponding author: Xin Dong

The research leading to these results has received funding from the Aerospace Technology Institute (UK) under Grant Agreement No. 102360 (FLARE) and from the Industrial Strategy Challenge Fund delivered by UK Research and managed by EPSRC under Grant Agreement No. EP/R026084/1 (RAIN).

[1]W. Ba, X. Dong, A. Mohammad, M. Wang and D. Axinte are with the Rolls-Royce UTC in Manufacturing and On-Wing Technology, University of Nottingham, NG8 1BB, UK

[2]Andy Norton is with Rolls-Royce plc, Derby, DE24 8BJ, UK

(E-mail: Weiming.Ba@nottingham.ac.uk; Xin.Dong@nottingham.ac.uk; Mingfeng.Wang@nottingham.ac.uk; Abd.Mohammad@nottingham.ac.uk; Dragos.Axinte@nottingham.ac.uk; Andy.Norton@Rolls-Royce.com).

the overall cable displacements [5], which can keep the maximum tracking error less than 3mm for a circular path. Further, more advanced control strategies were deployed to improve the control accuracy of PPC-based approaches. For instance, the fuzzy algorithm was utilized to learn the nonlinear model based on the Jacobian of multiple local operating points for path tracking on a tendon-driven 3-DoF extensible single-section continuum manipulator in [14], where the integral absolute error (IAE) was reduced from $0.3\mathrm{m}\cdot\mathrm{s}$ (Jacobian method) to $0.24\mathrm{m}\cdot\mathrm{s}$ (fuzzy controller) for tracking a 1cm long linear path within 40s while the targeting precision was decreased from 3.1mm (Jacobian method) to 0.72mm (fuzzy controller). Also, a hybrid position/force control was performed in [15] on a multi-backbone tendon-driven continuum robot using the Jacobian. Concurrently, beam theory [16] and cosserat rod theory [17] are applied to pursue more complex modelling approaches. However, the performance development is limited compared to the computational burden and estimation cost. In comparison, model-free control generally employs data-driven algorithms, most of which apply neural-network-based controllers to compensate for the errors caused by the hard-to-predict factors of continuum/soft robots. For example, neural network was utilised to learn the global IK for point-to-point Jacobian-based feedback control of a 405mm-long dual-module 6-DoF pneumatic manipulator with a mean error of 9.67mm [18]. Also, feed forward NN was used to approximate the inverse kinematic model of a soft manipulator [19]. Moreover, estimated Jacobian from sensor data was proposed in [20] for model-less hybrid position/force control of a multi-backbone tendon-driven continuum robot.

A great number of efforts have been made on studying different control approaches for continuum robots, most of which were conducted on short single section continuum robots. However, it is still challenging to achieve both rapid and accurate operation of multiple-section continuum robots. On the one hand, the learning-based open-loop approaches can realise rapid motion, but it is time-consuming to obtain the pre-trained model, and the accuracy largely relies on the repeatability of the robots. More importantly, those approaches have no resistance to external disturbances. On the other hand, for those closed-loop methods, most of them adopt the PCC assumption for kinematic modelling, regardless of the modelling error between the actual robot shape and the theoretical ones. While the model-free methods, either applying neural networks for feedforward control or advanced algorithms for reinforcement learning, require extra training for workspace calibration, which are difficult to be generalized to multi-section continuum robots, as the amount of the training dramatically increases from one to multiple sections. Moreover, those methods fail to consider the non-negligible cable elongations when the full length and tension of the driven cable becomes considerable, resulting in inaccuracy control of cable displacements. Considering the merits and demerits of both model-based and model-free methods, a novel model-less fuzzy-logic-based controller is developed in this work, which has following advantages: first of all, by utilizing the fuzzy logic algorithm, the control policies directly from task space to actuation space are obtained without the PCC assumption, avoiding the model mismatch issue for those CRs whose shape significantly deviate from the circular arc; secondly, formally the controller realizes the mapping from the positioning error to the increments of cable displacements, which is disturbance-free from external interference comparing to the pre-trained static models by model-free approaches.

The paper is organized as follows: Chapter II introduces an extra slender continuum robot, together with analysis of control challenges including PCC model failure, cable elongation and sections coupling. Then, a novel local fuzzy-logic-based model-less controller is proposed for accurate tip positioning of tendon-driven continuum robots in chapter III. In Chapter IV, a series of experiments on a single section are conducted to compare the proposed fuzzy-logic controller with the PCC-

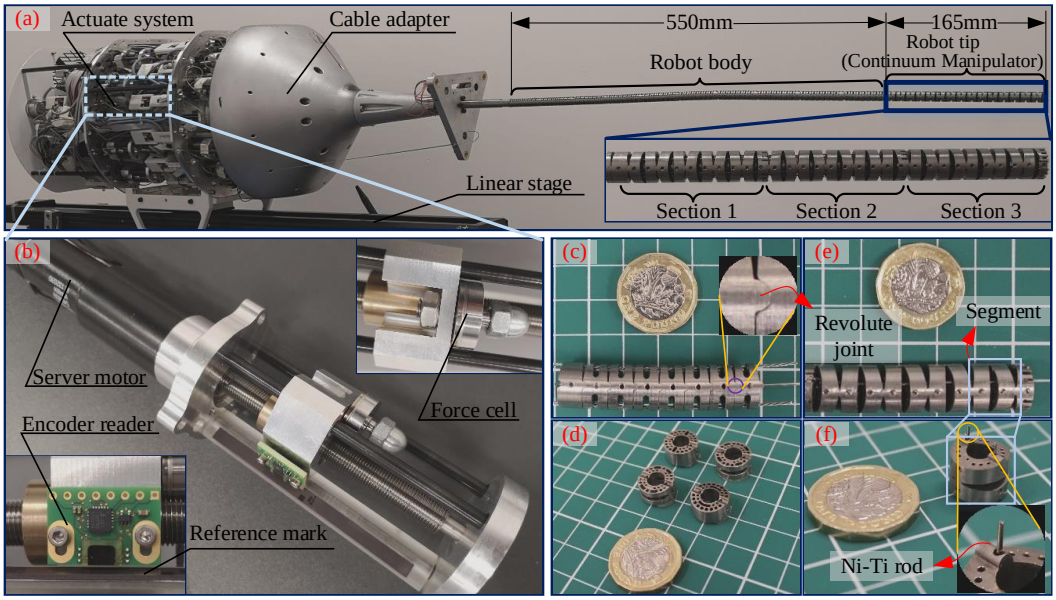

Fig. 1 Extra-slender robot system: (a) overall model of the continuum robot; (b) motor module with linear encoder, screw shaft and force cell; (c) single body section; (d) disk design for the continuum robot body; (e) single tip section; (f) disk design for the continuum robot tip

based approach and characterize its positioning performance. Additional trials on two sections are performed to explore the ability of the controller for the section coupling issue. Finally, Chapter V comes to the conclusions and further discussion.

II. Prototype Specification and Control Challenges

In this chapter, a unique slender continuum robot (length/diameter: 715mm/12.7mm) is introduced, including the mechanical design of the robotic arm and the actuation system. Then, the control challenges are presented mainly from three aspects, which are PCC model failure, cable elongation and section coupling.

A. Specification of the extra-slender continuum robot

As shown in Fig. 1(a), the prototype of the continuum robot is presented, which is designed for the in-situ maintenance of aeroengine combustors. The robot tip is composed of three 2-DoF sections (Fig. 1(e)) while the robot body contains ten 1-DoF sections (Fig. 1(c)). The robot body was designed for delivering the robot tip to desired locations in the combustor by following its inner chamber. The displacements of all the driven cables are controlled by 29 motor modules (Fig. 1(b)). Also, all the driven cables are dispersed by applying a 3D-printed cable adapter (Fig. 1(a)) to expand the space for the installation of motor modules. In addition, one linear stage is applied to deliver the whole robot into/out of the aeroengines during the navigation process.

In this system, the design combined of rigid revolute and compliant joints is utilized to provide compliant capability (Fig. 1(e) and (f)). The smallest recursive unit within one section is denoted by segment (Fig. 1(e)), which is composed of two disks. Every two adjacent disks are connected by one pair of short NiTi rods which pass through the through holes in the revolute joints and are locked by screws from the sides of the disks. One pair of compact semi-cylindrical groove and bulge between two disks makes up one revolute joint, contributing 1-DoF to the segment.

B. Control challenges for the tip section of the prototype

This paper focuses on the controller design for the tip sections of the proposed robot. The control challenges mainly come from two aspects. On the one hand, the shape of a single tip section significantly deviates from the circular arc, which brings in the model mismatch issue when applying PCC-based controllers and proposes requirements of model-less controllers. On the other hand, the section coupling issue, including kinematic and physical coupling, is a common challenge for the control of multi-sections, which is also an essential indicator to characterize the performance of a controller.

1) PCC assumption mismatch: in most of the existed research, each section of continuum robots is treated as a circular arc to describe the shape and to derive the kinematic model. The PCC assumption is widely utilized for controlling short continuum robots when the deviation between the actual shape of single section and the assumed circular arc is negligible or the accuracy requirement is not high. However, for the continuum robot proposed in this paper, there exists non-negligible deviation between the actual shape and the PCC-based model, which is called the PCC assumption mismatch and can be explained from two aspects. Firstly, given the same bending angle θ, the error between the PCC-based model and the geometry of the robot is obvious, which is shown in Fig. 2(a). Secondly, Fig. 2(b) reveals that segments within a single section are unevenly bent, which further contributes to the model mismatch issue.

It is demonstrated that the actual shape of the proposed robot does not comply with the PCC assumption. In fact, the PCC-based controller cannot keep convergent at all the target points within the workspace when applied on the robot owing to the mismatch issue, which was experimentally verified and presented in Section B of Chapter IV.

2) Section coupling: since the driving cables for the distal sections of continuum robots inevitably pass through the proximal ones, the coupling issue is brought in for the control of multi-section continuum robots, which leads to two major problems. (i) The first problem is the physical coupling, namely, the driving cables for the distal sections will apply extra torque and force on proximal sections. The physical coupling is the intrinsic property of tendon driven CRs, which has a great effect on the stability of multi-section system. (ii) The second problem is kinematic coupling. The total cable lengths for controlling the distal section (cable one: L_1+L_2; cable two: L_3+L_4) are determined by both proximal and distal sections. If there is a difference between the theoretical and actual pose of the proximal section, the lengths of the cables shaping the pose of the distal section (L_1' and L_3') will not equal to the theoretical values ($L_1$and L_3). Hence, the configuration of the distal section will be affected, regardless of its modelling accuracy. Obviously, the PCC assumption mismatch will be magnified on multiple sections because of the kinematic coupling issue.

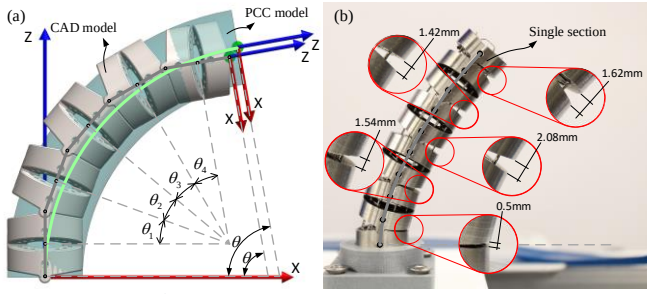

Fig. 2 Illustration of the PCC assumption mismatch issue: (a) Comparison of the PCC model and CAD model with the same bending angle θ; (b) One configuration of the robot depicting uneven bending of different segments within single section.

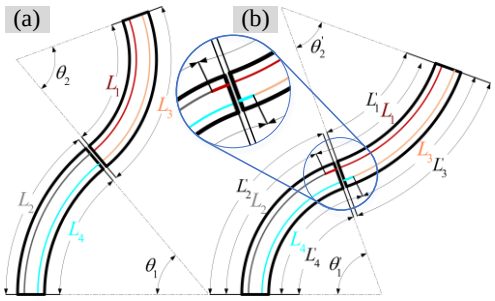

Fig. 3 Illustration of kinematic section-coupling issue (a) theoretical pose of two sections with bending angles (θ_1, θ_2); (b) actual pose with a control error ($\theta_1' > \theta_1$) on the base section.

In conclusion, the model-based approach is inappropriate to the proposed prototype owing to the PCC assumption mismatch, cable elongation and the kinematic coupling, while those model-free methods applying NN and reinforcement learning are time consuming for massive data sampling and model pretraining. Therefore, a model-less controller, which does not fully rely on kinematics, was developed by utilizing a fuzzy-logic algorithm to avoid the defects of both model-based and model-free methods, which was validated by the comparative experiments with the PCC-based approach.

III. Control Methodology

In this chapter, a novel local model-less feedback controller is developed to address the challenges presented in the previous chapters, by replacing the PCC assumption with a fuzzy-logic-based approach in the second stage of the control.

A. Framework of the control system

Fig. 4 shows the overall control architecture, which consists of two stages, a kinematics-based open-loop stage followed by a close-loop stage implemented by the proposed model-less controller. In the first stage, the desired position (x_d, y_d) is given as the system input, which is used to compute the desired cable displacements with the kinematic model developed in Section III-B. Once all the motors complete the displacements computed based on the kinematic model, the robot reaches a position close to the desired one; then the operation enters into the 2nd stage where the conventional PCC-based controller is substituted with a fuzzy-logic-based approach, leading the robot to the desired position with minimised positional error and preventing the non-convergent problem caused by PCC assumption mismatch (see details in Fig. 18).

B. Kinematics - the 1st stage of the control system

Usually, to describe the pose of single section accurately in the configuration space (like the joint space for conventional rigid-link manipulator), bending angle (θ) and direction angle (φ) are generally used to indicate the configuration of a single section, as shown in Fig. 5(b). Also, it can be found that in the conventional model-based kinematics, the configuration space (bending and direction angles θ and φ) is a bridge linking the task space (Fig. 5(a)) and actuation spaces (Fig. 5(c)) to build the kinematics model. The inverse kinematics from configuration space to actuation space is called robot-specific kinematics based on the geometry of the robot's structure to build the mapping from robot's shape to actuator length, which

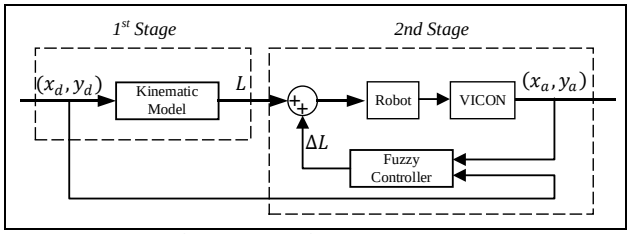

Fig. 4 Architecture of the control framework including two stages. The purpose of the first stage is to drive the robot tip close to the desired position so that the adjustments of cable displacements in the second stage can be reduced, which can lower the risk of over-tensioning or over-releasing the driving cables in the control process.

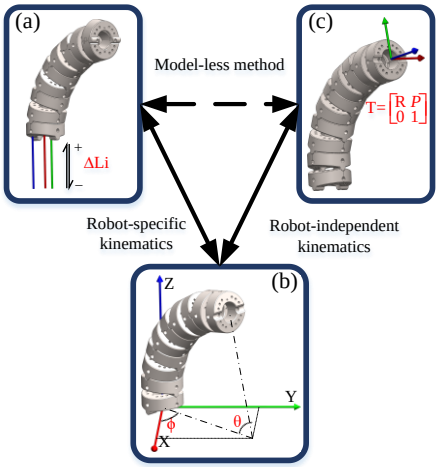

Fig. 5 Kinematic mapping between (a) actuation space, (b) configuration space and (c) task space. The model-based kinematics with PCC assumption consists of two parts: the robot-specific kinematics and the robot-independent kinematics, while other model-less methods establish control policies directly from task space to actuation space.

is regarded as the low-level control of the robot. The robot independent kinematics refers to the relationship between the configuration and task spaces, which combines the pose of every single section with the shape of the robot.

1) Robot-independent kinematics

Fig. 6 (c) shows the definition of all local coordinate systems attached on a single segment. In the figure, two coordinate systems (base and tip frames) are defined at the bottom and up surfaces of each disk.

The whole transformation process for a single segment is shown below:

$$XYZ_{1b} \xrightarrow{T_1} XYZ_{1t} \xrightarrow{T_2} XYZ_{2b} \xrightarrow{T_3} XYZ_{2t}$$

Then, the homogeneous transformation matrix (HTM) of a single segment can be written as below (Fig. 6(c)):

$$T_{seg} = T_1 T_2 T_3 \quad (1)$$

Since every single section is made up of five serially linked segments (Fig. 6(b)), the local HTM for section i can be derived as:

$$T^i_{b\to t} = [T_{seg}]^5 (i = 1,2,3) \quad (2)$$

Similarly, the global HTM could be obtained for each section in Fig. 6(a) relative to the world frame:

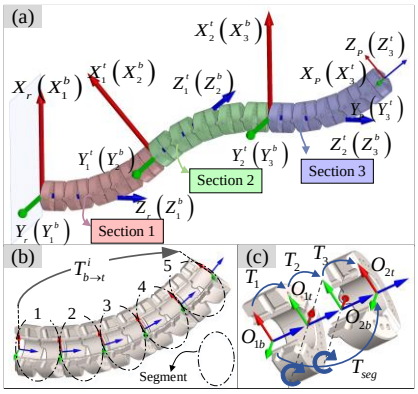

Fig. 6 Definition of coordinate systems for (a) three-section continuum manipulator; (b) a single section; (c) a single segment. (the axes in red, green and blue are X, Y and Z axes, respectively)

$$T^j = \prod_{j=1}^{3} T^i_{b\to t}\ (i = 1 \text{ to } 5, j = 1 \text{ to } 3) \quad (3)$$

2) Robot-specific kinematics

The kinematics from the configuration space to actuation one varies with each specific continuum robot. For the robot presented in this paper, a design of twin-pivot backbone is utilised to keep the whole structure compact. Disks with tilt faces are alternatively placed in 90° so that every single section can bend with 2-DoF in space.

Firstly, the cable displacement is derived for a single segment, for which the explicit structure is given in Fig. 7. Since the lengths of the cables within the disks keep constant, here only the lengths of those between gaps are considered in the kinematic model, which can be written as:

$$l^k_{i,j}(\beta_{k,1}, \beta_{k,2}) = {}^{gap1}_{l^k_{i,j}}(\beta_{k,1}) + {}^{gap2}_{l^k_{i,j}}(\beta_{k,2}) \quad (4)$$

where $\beta_{k,1}, \beta_{k,2}$ are the angle variations of gap 1 and 2, respectively, from the initial angle of both gaps β_0.

The explicit expressions of the cable lengths in gap 1 and 2, ${}^{gap1}_{l^k_{i,j}}(\beta_{k,1})$ and ${}^{gap2}_{l^k_{i,j}}(\beta_{k,2})$, respectively, are described in the following form:

$$\begin{aligned} {}^{gap1}_{l^k_{i,j}}(\beta_{k,1}) &= \frac{2r\sin\alpha^1_{i,j}}{\cos\beta_0}\sin\left(\beta_0 + \frac{\beta_{k,1}}{2}\right) \\ {}^{gap2}_{l^k_{i,j}}(\beta_{k,2}) &= \frac{2r\sin\alpha^2_{i,j}}{\cos\beta_0}\sin\left(\beta_0 + \frac{\beta_{k,2}}{2}\right) \end{aligned} \quad (5)$$

which r is the radius of the circle where the cable holes locate, $(\alpha^1_{i,j}, \alpha^2_{i,j})$ are single cable's phase angles in disk A and B.

The expression of cable length variations is given in (6) when the robot moves from the straight shape to the desired state:

$$\Delta l^k_{i,j} = l^k_{i,j}(\beta_{k,1}, \beta_{k,2}) - l^k_{i,j}(0,0) \quad (6)$$

Since $(\frac{\beta_{k,1}}{2}, \frac{\beta_{k,2}}{2}) \in$ [-5°, 5°], the following approximations are applied to (5):

$$\sin(\frac{\beta_{k,1}}{2}) \approx \frac{\beta_{k,1}}{2}, \sin(\frac{\beta_{k,2}}{2}) \approx \frac{\beta_{k,2}}{2}, \cos(\frac{\beta_{k,1}}{2}) \approx 1, \cos(\frac{\beta_{k,2}}{2}) \approx 1$$

Then, (6) can be simplified as:

$$\Delta l^k_{i,j} = c^1_{i,j}\beta_{k,1} + c^2_{i,j}\beta_{k,2}, (c^1_{i,j} = r\sin\alpha^1_{i,j}, c^2_{i,j} = r\sin\alpha^2_{i,j}) \quad (7)$$

Hence, the cable displacement in a single section composed of five segments can be obtained:

$$\Delta L^k_{i,j} = 5\Delta l^k_{i,j} \quad (8)$$

The matrix format of (8) is given below:

$$[\Delta L^k_i] = [C^k_i][\beta_k] \quad (9)$$

where $[\Delta L^k_i] = [\Delta L^k_{i,1} \quad \Delta L^k_{i,2} \quad \Delta L^k_{i,3}]^T$

$$[C^k_i] = 5\begin{bmatrix} c^1_{i,1} & c^2_{i,1} \\ c^1_{i,2} & c^2_{i,2} \\ c^1_{i,3} & c^2_{i,3} \end{bmatrix}, [\beta_k] = [\beta_{k,1} \quad \beta_{k,2}]^T.$$

Finally, it comes to the calculation of the overall length variations of the driven cables for section i, which can be written as:

$$[\Delta L_i] = \sum_{k=1}^{i}[\Delta L^k_i] = \sum_{k=1}^{i}[C^k_i][\beta_k] \quad (10)$$

C. Fuzzy-logic-based Controller - the 2nd stage

As mentioned in the control challenges of Chapter II, the model-mismatch issue makes conventional model-based controllers inappropriate for the robot developed in this research, whose actual shape deviates remarkably from a circular arc. Here, based on the analysis of the movement mechanism for tendon-driven CRs, a fuzzy logic algorithm is adopted to design the model-less feedback controller, which excludes the bending angle φ from the controller.

1) Preliminary motion analysis of a single section

Section movement mechanism: Even though the PCC assumption is widely adopted for the kinematics modelling of CRs, arc parameters (θ, φ) are dispensable for the derivation of feedback controllers. Inspired by the tug of war shown in Fig. 8(a), the movement of tendon driven CRs can be also seen as the tug among three driving cables (Fig. 8(b)). The control law in the tug of war is quite straightforward to keep the target point in the middle: when the target is bias towards one side, pull the rope on the other side. Likewise, similar control policies can be summarized to guide the displacements of three cables in a single section of a continuum robot, according to the error vector from actual position P_a to desired one P_d, which can minimise the kinematics error caused by cable elongation.

Section motion decomposition: Any pose transition between two different states of CRs can be regarded as the combination of two elementary motions (Fig. 9), namely, rotation about Z axis and movement within the bending plane where the robot locates. Similarly, the error between desired and actual poses of CRs can be decomposed into two independent components, which can be considered separately in the closed-loop control.

Hence, based on the above analysis, two independent fuzzy-logic controllers were developed for the positioning error

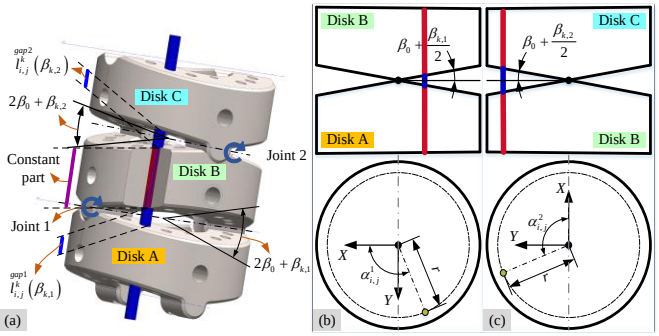

Fig. 7 Illustration of single driven cable (a) within one segment, (b) joint 1 between disk A and B, with its top view and (c) joint 2 between disk B and C, with its bottom view.

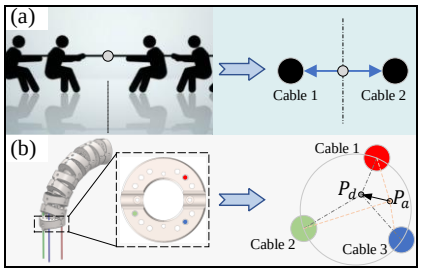

Fig. 8 Illustration of the movement mechanism of (a) the tug of war and (b) tendon-driven CRs. For a 2-DoF CR, the tip position control problem in 3D space can be regarded as the tug among three driving cables in a 2D plane, which avoids the model error caused by cable elongation when utilizing arc parameters (θ, φ) in the PCC model.

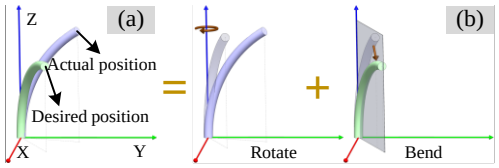

Fig. 9 Schematic diagram of motion decomposition for single section. (a) The expected adjustment from actual position to desired position can be divided into the combination of (b) rotary and bending motion.

reduction, which are noted as $Fuzzy_p$ (for the radial positioning error) and $Fuzzy_\varphi$ (for the angular positioning error).

2) Fuzzification and defuzzification

In the fuzzy controller design procedure, the first step is to realize the fuzzification of input variables and defuzzification of output variables.

By describing the tip position in a cylindrical coordinate system (Fig. 10(a)), the PCC-based kinematics from configuration space to task space given in [13] can be rewritten as below:

$$\begin{bmatrix} p \\ \varphi \\ z \end{bmatrix} = \begin{matrix} S \cdot \frac{1-\cos\theta}{\theta} \\ \phi \\ \lfloor\ S \cdot \frac{\sin\theta}{\theta}\ \rfloor \end{matrix} \tag{11}$$

Where S denotes the backbone length of a single section.

Since the single section is designed with 2-DoF for inextensible CRs, there are only two independent variables among (p, φ, z) in the task space. Actually, (p, φ) is the projection of the point (p, φ, z) on the bottom plane, which can realize full mapping from the spatial workspace to 2D plane. Therefore, the variable z will not be utilized in the controller design.

Fig. 10(b) plots the curve of ${}^{p}/_{S} = \frac{1-\cos\theta}{\theta}$ (red solid line) and the fitted line $y = k\theta (k = 0.44)$ (black dash line) when $\theta \in \left[0, \frac{\pi}{2}\right]$. It can be observed that $\frac{1-\cos\theta}{\theta}$ is approximately linear to θ. Hence, it can be concluded that the radial distance p is proportional with the bending angle θ with high linearity while the angular position φ coincides with the direction angle ϕ, the following relationships can be obtained:

$$\begin{matrix} p \propto \theta;\ \varphi \equiv \phi \\ dp \propto d\theta;\ d\varphi \equiv d\phi \end{matrix} \tag{12}$$

Equation (13) gives the vector form of the PCC-based kinematics from configuration space to actuation one:

$$L = S - r\theta\cos(\alpha - \phi) \tag{13}$$

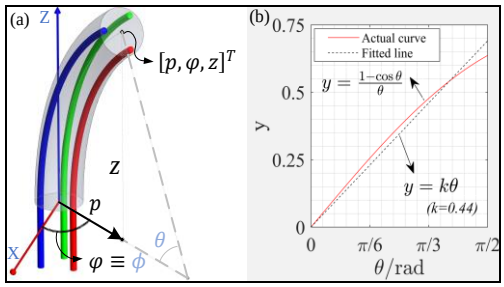

Fig. 10 (a) Schematics of the kinematic model; (b) the function of the quotient of the radial coordinate p and the backbone length S: ${}^{p}/_{S} = \frac{1-\cos\theta}{\theta}$. Here the cylindrical coordinate system $[p, \varphi, z]^T$ is applied to replace the Cartesian coordinate system $[x, y, z]^T$ in the task space.

Where L is the cable length within a single section, r denotes the distance from the robot centre to the driving cable, and α is the phase angle depicting the location of the driving cable (Fig. 7(b-c)).

The differential component of (13) to θ can be derived as below:

$$dL_\theta = -r\cos(\alpha - \phi) \cdot d\theta \tag{14}$$

Combining (12) and (14), it can be concluded that

$$dL_\theta \propto -\cos(\alpha - \varphi) \cdot dp \tag{15}$$

Equation (15) implies that given the increment $d\theta$, which is equivalent to dp according to (12), the cable displacement is the function of the angular position φ and the radial error increment dp. Hence, the expression of the first controller can be noted as $\Delta l_p = Fuzzy_p(\varphi_a, e_p)$, where φ_a denotes the actual angular position while e_p (Fig. 11(a)) is used to replace dp. Similarly, the expression of the second controller for minimising the angular position error component $p_d e_\varphi$ (Fig. 11(a)) can be obtained: $\Delta l_\varphi = Fuzzy_\varphi(\varphi_a, p_d e_\varphi)$. Therefore, the input variables for design of the fuzzy controllers are φ_a, e_p and $p_d e_\varphi$, excluding the arc parameters (θ and ϕ) from the controller. This addresses the nonconvergent problem of the positional control caused by PCC assumption mismatch, which is proved in Section B of Chapter IV.

The variation range of the angular position φ is defined to be the interval [-180°,180°), which covers the whole workspace and is in consistent with the function domain of $atan2(x, y)$. As shown in Fig. 11(b), the locations of the cable holes are selected in the whole range of φ to be the centre of 17 districts (N8-N1, S0, P1-P8). The triangular membership function (MF) in Fig. 11(c) is employed to describe the membership grades of certain points belonging to different districts. Further, the variation of the positional error components $e_p(mm)$ and $p_d e_\varphi(mm)$ in Fig. 11(b) is categorized into three ranges (Fig.

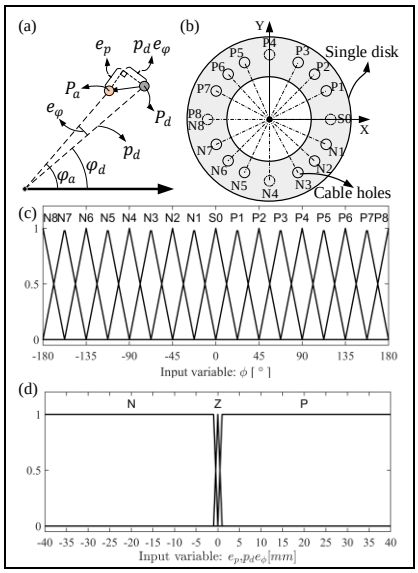

Fig. 11. (a) Error $(P_a - P_d)$ decomposition in the polar coordinate system, the error component in the radial direction is e_p while in the angular direction is $p_d e_\varphi$; (b) District divisions of a single section's workspace based on the distribution of cable holes in the X-Y plane; (c) MFs associated with the angular position φ; (d) MFs associated with the error components e_p and $p_d e_\varphi$.

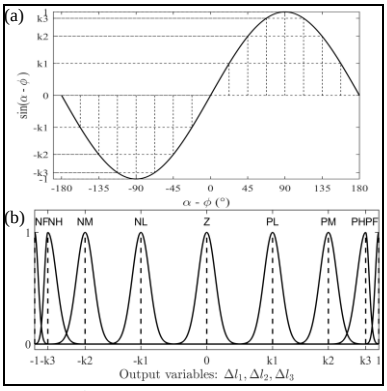

Fig. 12 (a) Trigonometric function utilized to determine the value of k_1, k_2 and k_3; (b) MFs utilized in the output variables Δl_1, Δl_2 and Δl_3 for both fuzzy controllers $Fuzzy_p$ and $Fuzzy_\varphi$.

11(d)), negative $(-\infty,-0.5]$, zero $[-0.5,+0.5]$ and positive $[+0.5,+\infty)$, which are noted using N, Z and P. Here the threshold value is set to be $0.5mm$, which can be adjusted according to the control accuracy requirement.

Owing to the axisymmetric and rotationally symmetric features for the distribution of cable holes, there are five different cable displacements in any elementary motions (Fig. 9), regardless of the cable moving directions. Those different cable displacements can be expressed as $\{0,\pm k_1,\pm k_2,\pm k_3,\pm 1\}$ by regularization in the interval of $[-1,1]$. Since the phase angle of the cable holes $\alpha \in \{-180°,-167.5°,\cdots,167.5°,180°\}$ and the angular position φ also belongs to the same set when the projection of the tip position locates at the centre of each district shown in Fig. 11(a), the variation range of $\alpha-\varphi$ can be determined, which is consistent with the range of α after regularization in the interval of $[-180°,180°]$. According to (15), the trigonometric function is utilized to determine the value of k_1, k_2 and k_3, which is shown in Fig. 12(a). The MFs of the outputs for both fuzzy controllers are depicted in Fig. 12(b), where the terms NF (negative full), NH (negative high), NM (negative medium), NL (negative low), Z (zero), PL (positive low), PM (positive medium), PH (positive high) and PF (positive full) denote $-1,-k_3,-k_2,-k_1,0,k_1,k_2,k_3,1$.

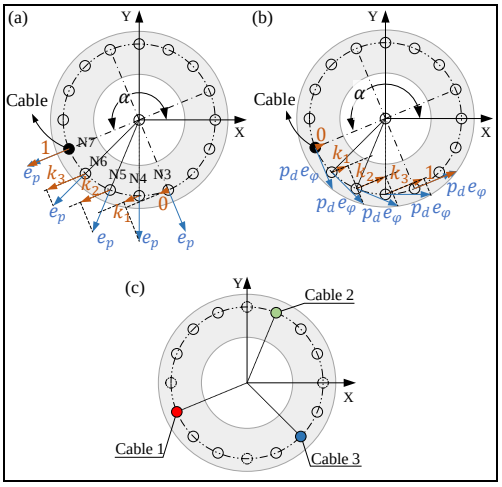

Fig. 13 Schematic diagram constructing the control policies of (a) $Fuzzy_p$ and (b) $Fuzzy_\varphi$ for the cable located at N7; (c) Cable distribution for Section 3.

3) Constructing of the fuzzy rules

In this part, the control rules are set up for a series of discretized points locating at the centre of different districts (N8-N1, S0, P1-P8), which is utilized to develop the nonlinear controllers $Fuzzy_p$ and $Fuzzy_\varphi$ by fuzzy-logic algorithm.

Without loss of generality, the cable at N7 (in Fig. 13), which doesn't locate on the X-axis or Y-axis, is selected to derive the control policies for both the position error components (e_p and $p_d e_\varphi$) in the polar coordinate system. As shown in Fig. 13 (a), the components (brown array) along the vector from the origin to the cable location varies when an identical radial error e_p (blue array) is given to the centre of different districts. It's feasible to empirically assume that the larger the component along the vector, the greater the cable displacement will be. If the maximum displacement, which is at N7, is regularized to be 1, then for N3-N6 the regularized cable displacements are $0,k_1,k_2,k_3$. Moreover, by the axisymmetric and rotational symmetric features of the robot structure, the regularized cable displacements can be derived based on N3-N7. The cases for cables at other locations can be analysed similarly. Therefore, the control policies of the first controller $Fuzzy_p$ for any cable

Table. I
The fuzzy rules for the first controller $\Delta l_p = Fuzzy_p(\varphi_a, e_p)$

φ_a	$e_p = N$			$e_p = Z$			$e_p = P$		
	Δl_p^1	Δl_p^2	Δl_p^3	Δl_p^1	Δl_p^2	Δl_p^3	Δl_p^1	Δl_p^2	Δl_p^3
N8	NH	PL	PM	Z	Z	Z	PH	NL	NM
N7	NF	PM	PL	Z	Z	Z	PF	NM	NL
N6	NH	PH	Z	Z	Z	Z	PH	NH	Z
N5	NM	PF	NL	Z	Z	Z	PM	NF	PL
N4	NL	PH	NM	Z	Z	Z	PL	NH	PM
N3	Z	PM	NH	Z	Z	Z	Z	NM	PH
N2	PL	PL	NF	Z	Z	Z	NL	NL	PF
N1	PM	Z	NH	Z	Z	Z	NM	Z	PH
S0	PH	NL	NM	Z	Z	Z	NH	PL	PM
P1	PF	NM	NL	Z	Z	Z	NF	PM	PL
P2	PH	NH	Z	Z	Z	Z	NH	PH	Z
P3	PM	NF	PL	Z	Z	Z	NM	PF	NL
P4	PL	NH	PM	Z	Z	Z	NL	PH	NM
P5	Z	NM	PH	Z	Z	Z	Z	PM	NH
P6	NL	NL	PF	Z	Z	Z	PL	PL	NF
P7	NM	Z	PH	Z	Z	Z	PM	Z	NH
P8	NH	PL	PM	Z	Z	Z	PH	NL	NM

Table. II
The fuzzy rules for the second controller $\Delta l_\varphi = Fuzzy_\varphi(\varphi_a, pe_\varphi)$

φ_a	$pe_\varphi = N$			$pe_\varphi = Z$			$pe_\varphi = P$		
	Δl_φ^1	Δl_φ^2	Δl_φ^3	Δl_φ^1	Δl_φ^2	Δl_φ^3	Δl_φ^1	Δl_φ^2	Δl_φ^3
N8	NL	PH	NM	Z	Z	Z	PL	NH	PM
N7	Z	PM	NH	Z	Z	Z	Z	NM	PH
N6	PL	PL	NF	Z	Z	Z	NL	NL	PF
N5	PM	Z	NH	Z	Z	Z	NM	Z	PH
N4	PH	NL	NM	Z	Z	Z	NH	PL	PM
N3	PF	NM	NL	Z	Z	Z	NF	PM	PL
N2	PH	NH	Z	Z	Z	Z	NH	PH	Z
N1	PM	NF	PL	Z	Z	Z	NM	PF	NL
S0	PL	NH	PM	Z	Z	Z	NL	PH	NM
P1	Z	NM	PH	Z	Z	Z	Z	PM	NH
P2	NL	NL	PF	Z	Z	Z	PL	PL	NF
P3	NM	Z	PH	Z	Z	Z	PM	Z	NH
P4	NH	PL	PM	Z	Z	Z	PH	NL	NM
P5	NF	PM	PL	Z	Z	Z	PF	NM	NL
P6	NH	PH	Z	Z	Z	Z	PH	NH	Z
P7	NM	PF	NL	Z	Z	Z	PM	NF	PL
P8	NL	PH	NM	Z	Z	Z	PL	NH	PM

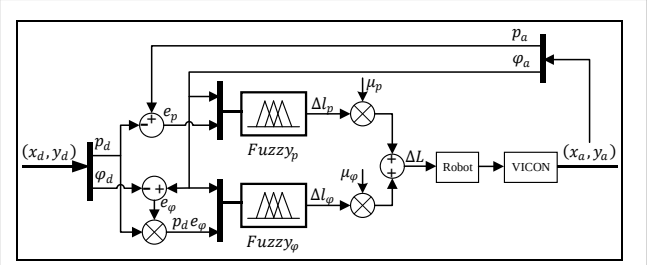

Fig. 14 Block diagram of the fuzzy-logic controller. The controller is made up of two sub-controllers, corresponding to the error correction in the radial and angular directions in the polar coordinate system.

can be obtained. Likewise, the same analysis method was applied for the derivation of the second controller ($Fuzzy_\varphi$).

Finally, based on the cable distribution of Section 3 in Fig. 13 (c), an example is given for the control policy construction of a single section, which is shown in Table. I and Table. II.

4) Integration of the fuzzy-logic controller

Fig. 14 illustrates the block diagram of the fuzzy-logic controller which integrates two sub-controllers together ($Fuzzy_p$ and $Fuzzy_\varphi$). The desired tip position (x_d, y_d) and the actual tip position (x_a, y_a) are converted to polar coordinates (p_d, φ_d) and (p_a, φ_a) to compute the radial position error $e_p = p_a - p_d$ and the angular position error $p_d e_\varphi = p_d(\varphi_a - \varphi_d)$. Then (φ_a, e_p) and $(\varphi_a, p_d e_\varphi)$ are utilized as the inputs of the 1st controller $\Delta l_p = Fuzzy_p(\varphi_a, e_p)$ and the 2nd controller $\Delta l_\varphi = Fuzzy_\varphi(\varphi_a, p_d e_\varphi)$. Since the outputs of both sub-controllers, Δl_p and Δl_φ, are regularized within $[-1,1]$, the coefficients μ_p and μ_φ are utilized to convert the outputs to the cable displacements. For simplicity, a fixed-step control is achieved by setting μ_p and μ_φ to be static ($\mu_p = \mu_\varphi = 0.01mm$) in this work, which can also be adjusted dynamically to be proportional to the value of e_p and $p_d e_\varphi$ to increase the speed of convergence.

Overall, in this chapter, instead of using PCC-based model in the entire controller, a fuzzy-logic-based algorithm is implemented in the second stage of the controller for point-to-point operation. The newly proposed model-less controller can address the challenges of PCC assumption mismatch, cable elongation and the multiple section kinematic coupling presented in chapter II, which was validated by a set of experiments shown in the next chapter.

IV. Experimental Validation

In this chapter, the proposed fuzzy-logic feedback controller has been implemented on the tendon-driven continuum robot introduced in Chapter II, whose actual shape deviates from the arc model, leading to the challenge of PCC assumption mismatch. Here, both the proposed controller and the PCC-based approach were implemented on a single section for evaluating the impact of the mismatch. Then, a set of points evenly distributed in the workspace were tested as the target position to characterize the overall positioning performance of the fuzzy-logic controller, thus the actual workspace of the single section was obtained. Besides, several trials applying the proposed controller on two sections were conducted to explore its capability for diminishing the section coupling issue.

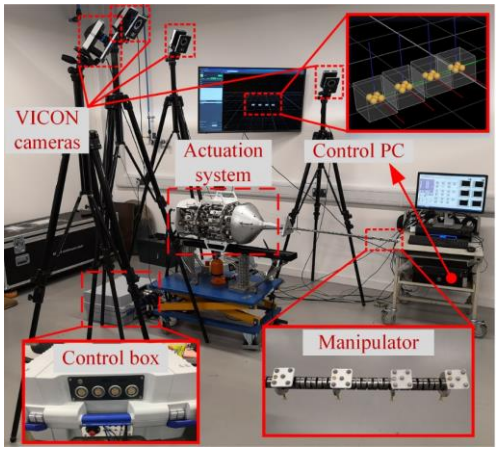

Fig. 15 Test-rig setup. The proposed controller is validated on the continuum manipulator with VICON as the feedback device.

A. Test-rig Setup

The setup of the test-rig is shown in Fig. 15. A 64-bit Windows 7 based computer with an Intel Xeon E5-1620 processor is used as the host controller to run the main control algorithm at an execution rate of 20 Hz using LabVIEW in 32-bit version. The experimental data (cable displacements, tip position) is also recorded at the same frequency. The desired cable displacements calculated by the host computer are sent to the sb-RIO board (National Instrument), which is utilised as the low-level controller for the closed-loop control of motors to realise precise displacements of all the driven cables. In addition, VICON system, is deployed to measure the tip position and orientation of each section, which is grasped and pre-processed by the program in 64-bit version LabVIEW running on the host computer. The measuring data is transferred from the 64-bit LabVIEW project to the 32-bit version control algorithm for the position feedback with a sampling rate of 100 Hz.

B. Experiments on Single Section

1) Experimental Comparison with the PCC-based Approach

To evaluate the proposed controller in aspect with the 1st control challenge (the PCC assumption mismatch) in Chapter II, the fuzzy-logic controller (Fig. 14) and the PCC-based one [21] (the gain factor is set to be 0.1 in the experiment), were implemented on single section of the prototype for comparison, both of which utilize VICON for sensory feedback. The average running time is benchmarked in LabVIEW with each controller running 10000 times iteratively, which is 1.85ms for the proposed controller and 0.67ms for the PCC-based one. Fig. 16 shows the 3D and 2D views of all the 17 target points used for the test, whose projections in the X-Y plane are evenly

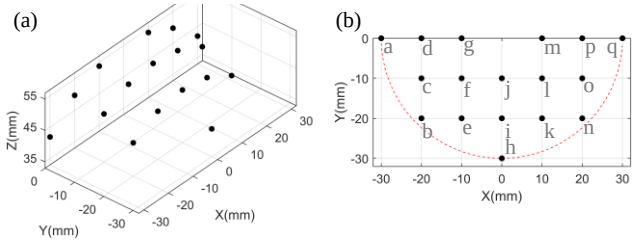

Fig. 16 Illustration of the target points for test. (a) 3D view and (b) Plane view.

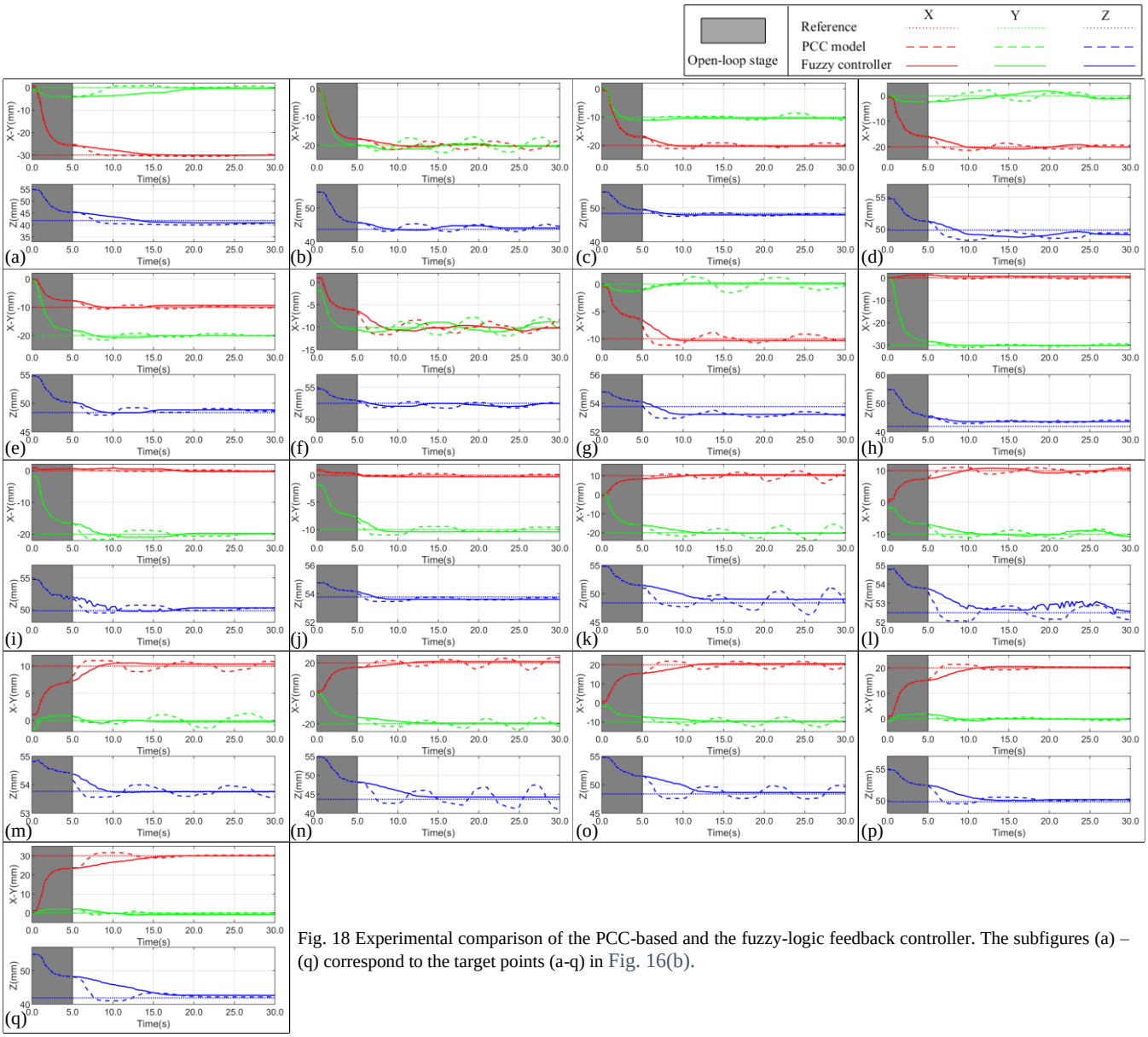

Fig. 18 Experimental comparison of the PCC-based and the fuzzy-logic feedback controller. The subfigures (a) – (q) correspond to the target points (a-q) in Fig. 16(b).

distributed within the semicircle in a radius of $30mm$ and centred at the origin. It is necessary to declare that the test zone is restricted to half of the workspace of the section (the 3rd and 4th quadrants) by the measuring range of the VICON system.

The performance comparisons between the fuzzy-logic and PCC-based controllers are illustrated in Fig. 18, where the subfigures (a)-(q) correspond to the target points (a-q) marked in Fig. 16b). Each subfigure depicts the actual Cartesian coordinates of the section tip in X (in red), Y (in green) and Z (in blue) axes in 30 seconds when the fuzzy-logic (in solid lines) and the PCC-based (dash lines) controller were implemented respectively with the open-loop stage shown in the grey area. It can be observed that the fuzzy-logic controller keeps converged at all the target points while the result of the PCC-based controller fluctuates at points b, d, f, g, k, l, m, n, and o.

Qualitative analysis for the oscillation of the PCC-based approach is that modelling error is imported when arc parameters (θ, ϕ) in configuration space are utilized as the intermediate to derive the control model from task space to actuation space based on the PCC assumption. As illustrated in the Section B of Chapter II, the PCC model cannot precisely describe the actual shape of the proposed robot. The experimental result reveals that the PCC-based controller takes effect at some target points. However, it cannot keep convergent for the target points in the whole workspace. In contrast, the proposed fuzzy-logic approach weakens the role of

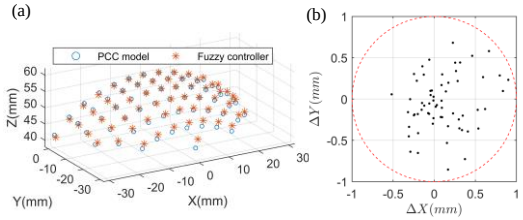

Fig. 17 (a) Comparison between theoretical PCC-based workspace and actual workspace measured by the fuzzy controller; (b) The scatter diagram showing the positioning accuracy of all the 63 testing points in the X-Y plane.

these parameters in the controller, rendering less modelling error introduced in the computation during operation. This enables the proposed controller can keep convergent for all the target points.

2) Overall Positioning Performance

In this test, the proposed controller is applied on a set of target points marked with blue circles in Fig. 17(a) to comprehensively characterize its positioning performance. Fig. 17(b) depicts the error map in both X and Y axes after the controller running for 20 seconds at every target point, which indicates that the overall positioning accuracy of the controller can reach $\pm 1mm$ in X and Y directions while for 75% points the positioning error can be kept within $0.5mm$ along both axes. After the test, the actual workspace was obtained, which is marked with red stars in Fig. 17(b). In addition, Fig. 17 shows that there exists remarkable offset in the Z axis between the PCC-based workspace and the actual workspace of the robot, demonstrating the PCC assumption mismatch.

C. Trials on Two Sections

Although the control performance and stability of the proposed controller has been validated on a single section, there still exists uncertainty whether it can take effect when applied on multiple sections owing to the section coupling issue presented in Chapter II. Hence, four trials on two sections have been conducted to research the effect of the controller on this issue. The target points configurations of both sections for the trails are given in Table. III.

Fig. 19(a)-(d) present the experimental results of Trials 1-4. The adjustment processes marked with yellow rectangle in (a) and (c) indicate that both sections affect each other during their motion to reduce the error under the control of the fuzzy controller and thus verify the existence of the kinematic section coupling issue, which also demonstrates the proposed controller can effectively reduce the positioning error (median positioning error: 0.7mm; minimal positioning error: 0.13mm) along X and Y axes in local coordinate system for both sections.

These trials demonstrate the efficacy of the proposed controller with respect to the kinematic section coupling issue. However, it should also be recognized that the performance of the proposed controller is greatly reduced (maximum positioning error: -2.17mm) by the physical coupling issue. A possible solution is to adopt the gradient stiffness of the robot along the length to physically reduce the interference between sections, which could be applied in the future design.

Table. III
Target points configuration for the trails on two sections

	Section 2			Section 3		
	X(mm)	Y(mm)	Z(mm)	X(mm)	Y(mm)	Z(mm)
Trial 1	10	-10	52.50	15	-15	49.10
Trial 2	10	-10	52.50	-15	-15	49.10
Trial 3	10	-20	48.38	15	-15	49.10
Trial 4	10	-20	48.38	-15	15	49.10

CONCLUSION AND FUTURE WORK

This paper presents a novel fuzzy-logic-based model-less feedback controller for tendon-driven continuum robots whose shape deviate from the PCC assumption. By utilizing the fuzzy logic algorithm, the controller successfully establishes the control policies from the task space to actuation space, realizing close-loop position control in task space and avoiding the PCC assumption mismatch issue of model-based methods.

The proposed fuzzy-logic controller was tested on a single section of the slender continuum robot, which can reach $\pm 1mm$ overall positioning accuracy and $\pm 0.5mm$ positional accuracy for 75% of the test points. As a comparison, a PCC-based controller was implemented and tested on the same prototype. The result shows the controller fails to converge at some of the testing points (12 out of 17) caused by the PCC assumption mismatch, verifying the PCC assumption mismatch issue on the prototype. Further, the controller was performed on two sections of the robot, demonstrating the capability of the controller on minimising the section coupling issue.

It is necessary to declare that this work focuses on the validation of the proposed novel controller. The open configuration of the experimental scenario is made to comply with the application condition of the VICON system, which is not identical with the practical application scenario.

Future work will include integrating tension supervision into the controller and testing the controller on a multi-section continuum robot with gradient stiffness design. A hybrid controller design integrating tension supervision/control will avoid the infeasible tension of driving tendons and improve the dynamic performance of the controller, while the gradient

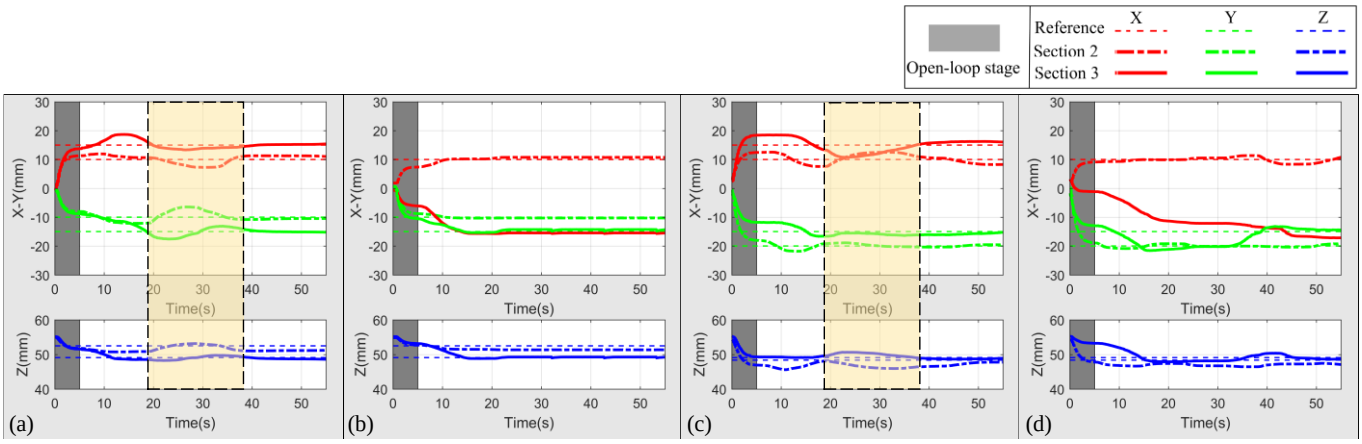

Fig. 19 Experimental results for (a) Trial 1, (b) Trial 2, (c) Trial 3 and (d) Trial 4.

stiffness design could efficiently solve the physical section coupling issue and the performance of the controller on multi-sections can be significantly improved.

ACKNOWLEDGMENT

The research leading to these results has received funding from the Aerospace Technology Institute (UK) under Grant Agreement No. 102360 (FLARE), China Scholarship Council (CSC) and University of Nottingham.

REFERENCES

[1] M. E. Giannaccini *et al.*, "Novel design of a soft lightweight pneumatic continuum robot arm with decoupled variable stiffness and positioning," *Soft Robot.*, vol. 5, no. 1, pp. 54-70, 2018.
[2] A. Melingui *et al.*, "Adaptive neural network control of a compact bionic handling arm," *IEEE/ASME Trans. Mechatronics.*, vol. 20, no. 6, pp. 2862-2875, 2015.
[3] M. Giorelli *et al.*, "Neural network and jacobian method for solving the inverse statics of a cable-driven soft arm with nonconstant curvature," *IEEE Trans. Robot.*, vol. 31, no. 4, pp. 823-834, 2015.
[4] Y. Kim *et al.*, "Active stiffness tuning of a spring-based continuum robot for MRI-guided neurosurgery," *IEEE Trans. Robot.*, vol. 34, no. 1, pp. 18-28, 2017.
[5] M. Li *et al.*, "Design and control of a tendon-driven continuum robot," *T I MEAS CONTROL*, vol. 40, no. 11, pp. 3263-3272, 2018.
[6] B. Ouyang *et al.*, "Design of an Interactive Control System for a Multisection Continuum Robot," *IEEE/ASME Trans. Mechatronics.*, vol. 23, no. 5, pp. 2379-2389, 2018.
[7] M. Wang *et al.*, "Design and development of a slender dual-structure continuum robot for in-situ aeroengine repair," *IROS*, pp. 5648-5653, 2018.
[8] M. S. Moses *et al.*, "Modeling cable and guide channel interaction in a high-strength cable-driven continuum manipulator," *IEEE/ASME Trans. Mechatronics.*, vol. 20, no. 6, pp. 2876-2889, 2015.
[9] Z. Du *et al.*, "Kinematics modeling and performance optimization of a kinematic-mechanics coupled continuum manipulator," *Mechatronics*, vol. 31, pp. 196-204, 2015.
[10] S. Satheeshbabu *et al.*, "Open Loop Position Control of Soft Continuum Arm Using Deep Reinforcement Learning," *ICRA*, pp. 5133-5139, 2019.
[11] B. A. Jones and I. D. Walker, "Practical kinematics for real-time implementation of continuum robots," *IEEE Trans. Robot.*, vol. 22, no. 6, pp. 1087-1099, 2006.
[12] R. J. Webster III and B. A. Jones, "Design and kinematic modelling of constant curvature continuum robots: A review," *Int. J. Robot. Res.*, vol. 29, no. 13, pp. 1661-1683, 2010.
[13] C. Escande *et al.*, "Kinematic calibration of a multisection bionic manipulator," *IEEE/ASME Trans. Mechatronics.*, vol. 20, no. 2, pp. 663-674, 2015.
[14] P. Qi *et al.*, "Kinematic control of continuum manipulators using a fuzzy-model-based approach," *IEEE T. Ind. Electron.*, vol. 63, no. 8, pp. 5022-5035, 2016.
[15] A. Bajo and N. Simaan, "Hybrid motion/force control of multi-backbone continuum robots," Int. J. Robot. Res., vol. 35, no. 4, pp. 422–434, 2016.
[16] Gravagne *et al.*, "Large deflection dynamics and control for planar continuum robots," *IEEE/ASME Trans. Mechatronics.*, vol. 8, no. 2, pp. 299-307, 2003.
[17] Trivedi *et al.*, "Geometrically Exact Models for Soft Robotic Manipulators," *IEEE Trans. Robot.*, vol. 24, no. 4, pp. 773-780, 2008.
[18] T. George Thuruthel *et al.*, "Learning closed loop kinematic controllers for continuum manipulators in unstructured environments," *Soft Robot.*, vol. 4, no. 3, pp. 285-296, 2017.
[19] M. Giorelli *et al.*, "A feed-forward neural network learning the inverse kinetics of a soft cable-driven manipulator moving in three-dimensional space," *IROS*, pp. 5033-5039, 2013.
[20] M. C. Yip and D. B. Camarillo, "Model-Less Hybrid Position/Force Control: A Minimalist Approach for Continuum Manipulators in Unknown, Constrained Environments," *IEEE Robot. Autom. Lett.*, vol. 1, no. 2, pp. 844-851, 2016.
[21] Penning, R. S. *et al.*, "An evaluation of closed-loop control options for continuum manipulators," *ICRA*, pp. 5392-5397, 2012.

Weiming Ba received the B.Eng. degree in Measuring and Control Technology and Instrumentation from Huazhong University of Science and Technology, Wuhan, China, in 2015.

He is currently working towards the PhD degree in Robotics for In-Situ Repair, Rolls-Royce University Technology Centre (UTC) in Manufacturing and On-wing technology, University of Nottingham. His research interests include modelling, analysis and control of continuum robots.

Xin Dong received his B.Eng. degree in Mechanical Engineering from Dalian University of Technology, Dalian, China, in 2008, the M.Eng and Ph.D. degrees.in Mechatronics, Robotics, and Automation Engineering from Beihang University, Beijing, China, in 2011 and from University of Nottingham, Nottingham, UK, 2015.

He is currently an Assistant Professor working at the University of Nottingham. His research interests are extra slender continuum robot and reconfigurable hexapod robots with novel actuation solutions for the application in Aerospace, Nuclear, Oil & Gas, Marine and rescue.

Abdelkhalick Mohammad received his B.Sc. degree in mechatronics engineering from Assiut University, Assiut, Egypt, in 2006, and the M.Eng. and Ph.D. degrees in robotics and mechatronics from Toyohashi University of Technology, Toyohashi, Japan, in 2010 and 2013, respectively.

He is currently an Assistant Professor in Mechatronics with the Department of Mechanical, Materials and Manufacturing Engineering, University of Nottingham, UK. His research interests include mechatronics system design, robotics, machine tool control, and control theory.

Mingfeng Wang (M'18) received the B.Eng. degree in mechanical design and automation and the M.Eng. degree in mechanical engineering from Central South University, Changsha, China, in 2008 and 2012, respectively, and the Ph.D. degree in mechanical engineering from University of Cassino and South Latium, Italy, in 2016.

He is currently a Research Fellow at Rolls-Royce University Technology Centre (UTC), University of Nottingham, UK. His research interests cover humanoid robots, precision farming robots, continuum robots.

Dragos Axinte is Professor of Manufacturing Engineering in the Faculty of Engineering, University of Nottingham. He is Fellow of the Institution of Mechanical Engineer (IMechE) and Fellow of the International Academy of Production Engineering (FCIRP). Since 2009 he is the Director of the Rolls-Royce UTC in Manufacturing and On-Wing Technology. He is also Editor-in-Chief of the International Journal of Machine Tools and Manufacture.

Andy Norton received his M.Sc. degree in Natural Sciences from University of Cambridge, Cambridge, UK, in 2009 and the Ph.D. degree in Materials from University of Oxford, Oxford, UK, in 2013.

He is currently an In-Situ Repair Technologist at Rolls-Royce plc. and project managing the development of novel systems to perform inspection and repair inside aeroengines, involving collaborations with a number of Rolls-Royce UTCs and Small/Medium-Sized Enterprises, as well as utilising a global Research & Development supply chain network.